JP

Research Publisher
Discovery that Matters

Adel Z. EL Dein

JOURNAL OF PHYSICS VOL. 1 NO. 2 July (2012) PP. 11 - 23

The Effects of the Span Configurations and Conductor Sag on the Magnetic-Field Distribution under Overhead Transmission Lines

Adel Z. El Dein

***Abstract*— Ground level electric and magnetic-fields from overhead power transmission lines are of increasingly important considerations in several research areas due to their impact on health and environmental issues. The paper presents a more generalized technique to calculate the magnetic-field generated by power transmission lines in three dimension coordinates. This technique has been evolved, formulated, analyzed and applied to a suggested 500-kV single circuit transmission line to evaluate the effects of line topology and terrain topography on the computed magnetic-field. The results are compared with two-dimensions technique.**

Keywords; OHTL, Magnetic-field, Sag Effect

I. INTRODUCTION

PRECISE analytical modeling and quantization of electric and magnetic-fields produced by overhead power transmission lines are important in several research areas [1]-[3]. Considerable research and public attention concentrated on possible health effects of extremely low frequency (ELF) electric and magnetic-fields [4-5]. An analytical calculation of the magnetic-field produced by electric power lines is produced in [6] and [7], which is suitable for flat, vertical, or delta arrangement, as well as for hexagonal lines. Also the estimation of the magnetic-field intensity at locations under and far from the two parallel transmission lines with different design arrangements is presented in [8]. The effects of conductors sag on the spatial distribution of the magnetic-field are presented in [9], in case of equal heights of the towers, equal spans between towers and the power transmission lines' spans being always parallel to each others.

In this paper, the magnetic-field is calculated by two different techniques; 2-D straight line technique and 3-D integration technique, where the effect of the sag in the magnetic-fields calculation, and the effects of unequal span distances between the towers, unequal towers heights, and when the power transmission lines' spans are not in straight line are investigated. The proposed three-dimension integration technique has been applied to different cases in order to justify its generalization for magnetic-field produced by actual transmission line configuration, arrangement, and terrain topography, and also has been applied to a suggested 500-kV single circuit overhead transmission line as an application case study.

II. MAGNETIC FIELD CALCULATIONS

A- The 2-D Straight-Line Technique

The common practice is to assume that power transmission lines are straight horizontal wires of infinite length, parallel to a flat ground and parallel with each other. This is a 2-D straight line technique, which can be found in many references [7-10]. In this paper, the vector magnetic potential approach combined with the superposition technique is used for the magnetic field calculations. This approach is considered as one of the efficient and straightforward techniques used for magnetic field calculation under OHTLs. It requires only physical parameters having specific values. The technique has been extended recently as a new approach for determining the magnetic field distribution of multiphase ac power TLs comprising multi-conductors [11-12]. The concept of this technique is based on the field theory of the infinite length two

Manuscript received May 15, 2012 and accepted June 5, 2012.

Electrical Engineering Dept., Faculty of Energy Engineering, South Valley University, Aswan 81528, Egypt. E-mail: azeinm2001@hotmail.com.

parallel wires shown in Fig. 1. It can be shown that the vector magnetic potentials A_{Z1} and A_{Z2} at the point (*x, y, 0*) from conductors 1 and 2 are, respectively:

$$A_{z1} = \frac{\mu o}{2\pi}[I\angle 0 \ln\{z_1 + [(x-x_1)^2 + (y-y_1)^2 + z_1^2]^{1/2}\}]_0^L \quad (1)$$

$$A_{z2} = \frac{\mu o}{2\pi}[I\angle 180 \ln\{z_2 + [(x-x_2)^2 + (y-y_2)^2 + z_2^2]^{1/2}\}]_0^L \quad (2)$$

In the previous equations, *I* and *-I* are expressed by $I\angle 0°$ and $I\angle 180°$, respectively and the variables *x, y* and *z* represent the coordinates of any point in the space around where the magnetic field is to be calculated.

Since 3-phase power TLs carry practically balanced currents, (1) and (2) can be extended to be applied for TLs of N conductors, each is carrying current *I*. In this case, the balanced currents can be expressed as $I\angle\theta_1$, $I\angle\theta_2$, $I\angle\theta_3$,……., $I\angle\theta_N$, such that:

$$I\angle\theta_1 + I\angle\theta_2 + I\angle\theta_3 + ... + I\angle\theta_N = 0 \quad (3)$$

From equations (1) and (3), the total vector magnetic potential from the ac N-conductor TL as *L* approaches infinity, can be expressed as:

$$A_{z_{Ac}} = \frac{\mu o}{2\pi}(\infty)\sum_{i=1}^{N}(I\angle\theta_i) - \frac{\mu o}{4\pi}\sum_{i=1}^{N}(I\angle\theta_i)\ln[(x-x_i)^2 + (y-y_i)^2] \quad (4)$$

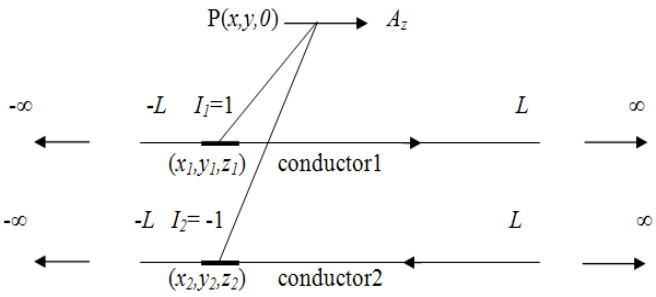

Fig. 1 Two-wire transmission line in the x-y plane

Therefore, the ac magnetic field components can be calculated using the expression for curl in Cartesian coordinates, as follow:

$$H_x = \frac{\partial A_z}{\partial y} = \frac{-I}{2\pi}\sum_{i=1}^{N}\left[\frac{(y-y_i)\angle\theta_i}{(x-x_i)^2 + (y-y_i)^2}\right] \quad (5)$$

$$H_y = \frac{\partial A_z}{\partial x} = \frac{-I}{2\pi}\sum_{i=1}^{N}\left[\frac{(x-x_i)\angle\theta_i}{(x-x_i)^2 + (y-y_i)^2}\right] \quad (6)$$

For ac applications, the currents of the 3-phase transmission line conductors are of the form:

$$I_1(t) = I_m \sin(\omega t) \quad (7)$$

$$I_2(t) = I_m \sin(\omega t + 120^\circ) \quad (8)$$

$$I_3(t) = I_m \sin(\omega t + 240^\circ) \quad (9)$$

This can be put in a phasor form as:

$$I_1 = \left(\frac{I_m}{\sqrt{2}}\right)\angle 0^\circ = I_{RMS}\angle 0^\circ \quad (10)$$

$$I_2 = \left(\frac{I_m}{\sqrt{2}}\right)\angle 120^\circ = I_{RMS}\angle 120^\circ \quad (11)$$

$$I_3 = \left(\frac{I_m}{\sqrt{2}}\right)\angle 240^\circ = I_{RMS}\angle 240^\circ \quad (12)$$

Hence, the total magnetic flux at any point will be consisting of a sinusoidal component, which can be represented as:

$$H_x = H_{x_{ac}} \cos(\omega t + \alpha) \quad (13)$$

$$H_y = H_{y_{ac}} \cos(\omega t + \beta) \quad (14)$$

Where ω is the angular frequency of the ac field and α and β are the phase angles of the two space fields.

The RMS values of the space components of the magnetic field are given by:

$$H_{i_{RMS}} = \sqrt{(H_x)^2 + (H_y)^2} \quad (15)$$

Research Publisher
Discovery that Matters

Adel Z. EL Dein **JOURNAL OF PHYSICS VOL. 1 NO. 2 July (2012) PP. 11 - 23**

Therefore, if the ac currents are applied in their phasor and RMS values, the RMS values of the ac magnetic field components over one ac supply cycle will be obtained.

B- The 3-D Integration Technique

In fact, the power transmission lines are nearly erected in periodic catenaries, the sag of each depends on individual characteristics of the line and on terrain topography conditions. The integration technique, which has been established in [13] and will be revealed here, is a three-dimensional technique which views the power transmission conductor as a catenary. In the integration technique, if the currents induced in the earth are ignored, then the magnetic-field of a single current-carrying conductor at any point P(x_o,y_o,z_o) shown in Fig. 2 can be obtained by using the Biot-Savart law [7-10], as:

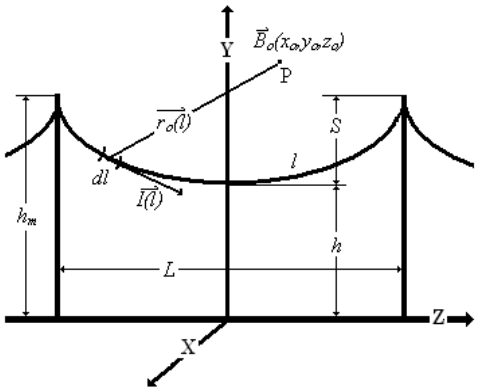

Fig. 2. Application of the Biot-Savart law

$$\vec{B}_o = \mu_o \int_l \frac{\vec{I}(l)dl \times \vec{a}_o(l)}{4\pi |\vec{r}_o(l)|^2} \tag{16}$$

where

l a parametric position along the current path,

$\vec{I}(l)$ the line current,

$\vec{r}_o(l)$ a vector from the source point (x,y,z) to the field point (x_o,y_o,z_o),

$\vec{a}_o(l)$ unit vector in the direction $\vec{r}_o(l)$, and

dl a differential element at the direction of the current.

The exact shape of a conductor suspended between two towers of equal height can be described by such parameters; as the distance between the points of suspension span L, the sag of the conductor S, the height of the lowest point above the ground h, and the height of the highest point above the ground h_m, where h_m-h=S. These parameters can be used in different combinations. Only two parameters are needed in order to define the shape of the catenary (S and L), while the third one (h or h_m), determines its location in relation to the ground surface. Fig. 3 depicts the basic catenary geometry for a single-conductor line, this geometry is described by:

$$y = h + 2\alpha \sinh^2(\frac{z}{2\alpha}) \tag{17}$$

where α is the solution of the transcendental equation: $2u(h_m - h)/(L) = \sinh^2(u)$; with $u = L/(4\alpha)$

The parameter α is also associated with the mechanical parameters of the line: $\alpha = T_h / w$ where T_h is the conductor tension at midspan and w is the weight per unit length of the line.

1) Case (A)

Fig. 2 illustrates the transmission line configuration, which gives the designation of Case (A), in which the power transmission lines are specified by, equal heights of the towers, equal spans between towers ($L1$=$L2$=L), and the power transmission lines' spans that are always parallel to each others. For a single span. the single catenary L is represented by Eq. (3). Since the modeled curve is located in the y-z plane, the differential element of the catenary can be written as:

$$d\vec{l} = dy\vec{a}_y + dz\vec{a}_z \tag{18}$$

$$d\vec{l} = dz(\frac{dy}{dz}\vec{a}_y + \vec{a}_z) \tag{19}$$

$$d\vec{l} = dz(\sinh(\frac{z}{\alpha})\vec{a}_y + \vec{a}_z) \tag{20}$$

$$\vec{r}_o = (x_o - x)\vec{a}_x + (y_o - y)\vec{a}_y + (z_o - z)\vec{a}_z \tag{21}$$

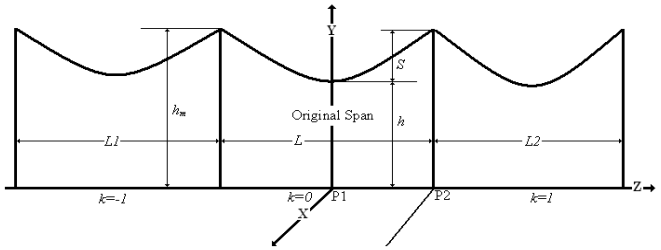

Fig. 3. Linear dimensions which determine parameters of the catenary.

where point (x_o,y_o,z_o) is the field point at which the field will be calculated, and point (x,y,z) is any point on the conductor catenary. Now, by substituting Eqs. (20) and (21) into (16),

and carrying out the cross product, the result at any point (x_o,y_o,z_o) is :

$$\vec{H}_o=\frac{\vec{I}}{4\pi}\int_{-L/2}^{L/2}\begin{pmatrix}[[(z-z_o)\sinh(\frac{z}{\alpha})-(y-y_o)]\vec{a}_x+\\(x-x_o)\vec{a}_y-(x-x_o)\sinh(\frac{z}{\alpha})\vec{a}_z]/d\end{pmatrix}dz \quad (22)$$

where:

$$d=[(x-x_o)^2+(y-y_o)^2+(z-z_o)^2]^{3/2} \quad (23)$$

This result can be extended to account for the multiphase conductors in the support structures. For (M) individual conductors on the support structures, the expression for the total magnetic-field becomes:

$$\vec{H}_o=\frac{1}{4\pi}\sum_{i=1}^{M}\sum_{k=-N}^{N}\int_{-L/2}^{L/2}(H_x\vec{a}_x+H_y\vec{a}_y+H_z\vec{a}_z)dz \quad (24)$$

where:

$$H_x=\frac{I_i[(z-z_o+kL)\sinh(\frac{z}{\alpha})-(y-y_o)]}{d_i} \quad (25)$$

$$H_y=\frac{I_i(x-x_o)}{d_i} \quad (26)$$

$$H_z=\frac{-I_i(x-x_o)\sinh(\frac{z}{\alpha})}{d_i} \quad (27)$$

$$d_i=[(x-x_o)^2+(y-y_o)^2+(z-z_o+kL)^2]^{3/2} \quad (28)$$

The parameter (N) in Eq. (24) represents the number of spans to the right and to the left from the generic one, as explained in Fig. 3. One can take into account part of the magnetic-field caused by the image currents. The complex depth ζ of each conductor image current can be found as given in [9-10].

$$\zeta=\sqrt{2}\ \delta\ e^{-j\pi/4} \quad (29)$$

where;

δ the skin depth of the earth represented by [10];

$$\delta=503\sqrt{\rho/f} \quad (30)$$

ρ the resistivity of the earth in Ω.m,

f the frequency of the source current in Hz.

The resultant magnetic-field with the image currents taken into account is also represented by Eq. (24), but its components will change and take the following formulas:

$$H_x=\frac{I_i[(z-z_o+kL)\sinh(\frac{z}{\alpha})-(y-y_o)]}{d_i}-\frac{I_i[z-z_o+kL)\sinh(\frac{z}{\alpha})-(y_o+y+\zeta)]}{d_i^{`}} \quad (31)$$

$$H_y=\frac{I_i(x-x_o)}{d_i}-\frac{I_i(x-x_o)}{d_i^{`}} \quad (32)$$

$$H_z=\frac{-I_i(x-x_o)\sinh(\frac{z}{\alpha})}{d_i}+\frac{I_i(x-x_o)\sinh(\frac{z}{\alpha})}{d_i^{`}} \quad (33)$$

$$d_i^{`}=[(x-x_o)^2+(y+y_o+\zeta)^2+(z-z_o+kL)^2]^{3/2} \quad (34)$$

This method can be applied at any field point above or near the earth's surface.

2) Case (B)

In Case (B), the power transmission lines are specified by, equal heights of the towers, equal spans between towers, and the power transmission lines' spans that are not parallel to each others. Each of the two catenaries *L* and *L2* in Fig. 4, has its original point and coordinate system. To calculate the magnetic-field intensity at any field point, this field point should be located in the coordinate system of the catenary under calculation.

Consider the field points of those that are located on X axis of the coordinate system (X,Y,Z) of the *L* catenary (P1 is the original point for this system). Those field points should be transferred to the coordinate system of the catanery under calculation. By applying this rule on field points and caterany *L*, it is seen that the same equations of case (A) are used, where the field points are already presented in caterany *L* coordinate system. But for caterany *L2*, the field points should be transferred to the caterany *L2* coordinate system.

Research Publisher
Discovery that Matters

Adel Z. EL Dein

JOURNAL OF PHYSICS VOL. 1 NO. 2 July (2012) PP. 11 - 23

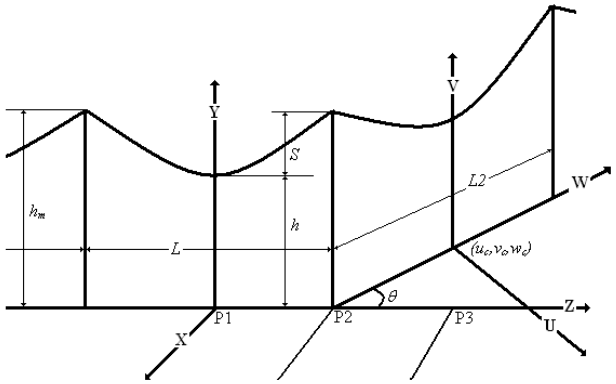

Fig. 4. Presentation of Case (B)

For any field point (x_1,y_1,z_1), this can be done in three steps:

1- Transfer the original of caterany *L2* (u_c,v_c,w_c) to the field point system. From Fig.(3), for $-90<\theta<90$

$z_c = dis + \frac{L2}{2}\cos(\theta)$, $x_c = \frac{-L2}{2}\sin(\theta)$, and $y_c = 0$

where; dis is the distance between the nearest point of catenary *L2* (point P2) and the original point of the field points' system. The distance dis changes with the location of the original point of the field points' system, e.g. when the original of the field points' system located at point P1; $dis = L/2$. Otherwise when the original of the field points' system located at point P2; $dis = 0$, and so on.

2- Transfer the field point (x_1,y_1,z_1) from its system to the system (U,V,W) of the caterany under calculation *L2*, from appendix (A):

$$w_1 = \frac{z_1 - z_c}{\sin(\beta+\theta)}\sin(\beta),\ u_1 = \frac{x_1 - x_c}{\cos(\beta+\theta)}\cos(\beta), \text{ and}$$

$v_1 = y_1 - y_c$, where (x_c,y_c,z_c) is the original point of system (U,V,W) refer to system (X,Y,Z), which is calculated in step (1), and $\beta = \tan^{-1}\frac{z_1 - z_c}{x_1 - x_c} - \theta$

3- Finally, use this point (u_1,v_1,w_1) in the same equations of case (A).

By using the superposition technique, the magnetic-field intensity at any field point above or near the earth's surface from many catenaries can be calculated.

3) Case (C)

In Case (C), the power transmission lines are specified by, unequal heights of the towers, unequal spans between towers, and the power transmission lines' spans that are always parallel to each others.

Fig. 5 presents a catenary *L1*, which has unequal heights of its towers (h_{m1},h_{m2}). In this case, α is the solution of the transcendental equation:

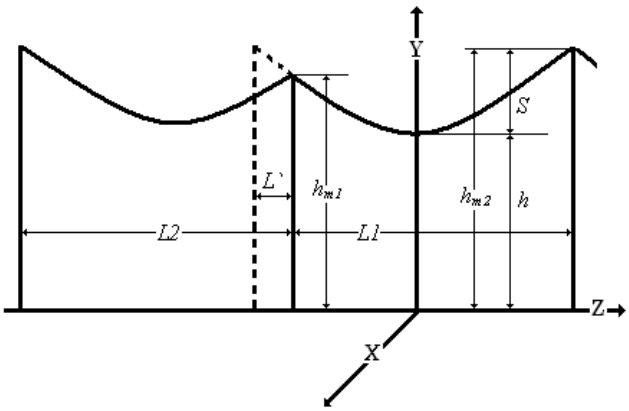

Fig. 5. Presentation of Case (C)

$2\frac{h_{m2}-h}{L1+L`}u = \sinh^2(u)$, with $u = \frac{L1+L`}{4\alpha}$ and the same equations as in case (A) is used, with the integration limits from $\frac{-L1-L`}{2}+L`$ to $\frac{L1+L`}{2}$.

Where $L`$ is the difference between the span length when equal heights of towers and that when there are unequal heights of towers.

Again, this method can be applied at any field point above or near the earth's surface.

III. Analysis of Magnetic-Fields Techniques

To calculate the Magnetic-field intensity at points one meter above ground level, under 500-kV transmission-line single circuit, which are presented in Fig.5, the data in appendix (B) are used. The phase-conductor currents are defined by a balanced direct-sequence three-phase set of 50Hz sinusoidal currents, with 2-kA rms.

Fig. 6 shows the computed magnetic-field intensity and its components by using the 2-D straight line technique, where the average heights of the transmission lines are used. It is noticed that the magnetic-fields intensity in this case have only two components H_x and H_y, and the longitudinal component H_z didn't appear. Fig. 7 shows the absolute value of each phase contribution in the Y-component of the magnetic-field intensity. It is noticed that the contribution of each phase is symmetrical around its phase position and the contribution of phases (1) and (3) make drop in the Y-component of the magnetic-field intensity nearly at -19m and 19m from the

center phase. Figs. 8 and 9 show the computed magnetic-field intensity and its components under a single span at both the midspan (at the maximum sag, point P1) and tower height (at point P2), and a distance away from the center phase as shown in Fig. 3, respectively, by using the 3-D integration technique (case A). It is noticed that the longitudinal components H_z appear and have a very small values.

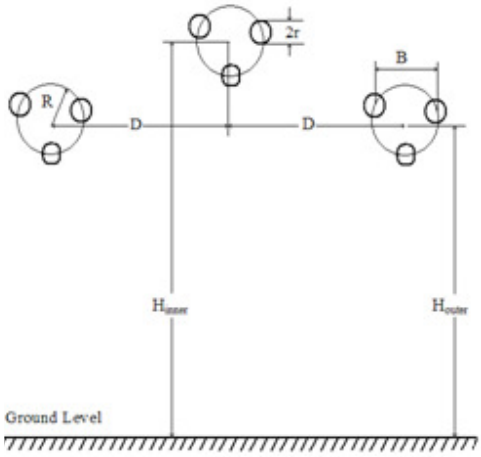

Fig. 6. Geometric presentation of 500-kV TL

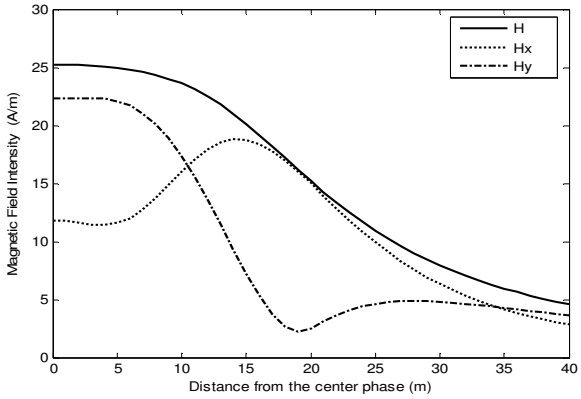

Fig. 7. Computed magnetic-field intensity by using the 2-D straight line technique.

Fig. 11 shows the effect of the number of spans (*N*) on the calculated magnetic-field intensity. It is noticed that, when the magnetic-field intensity is calculated at point P1 (Fig.3) and a distance away from the center phase, the effect of the spans' number is very small due to the symmetry of the spans around the field points, as explained in Fig. 3, where the contributions of the catenaries *L1* and *L2* are equal and smaller than the contribution of the catenary *L*, since they are far from the field points. But when the magnetic-field intensity is calculated at point P2 (Fig.3) and a distance away from the center phase, the effect of the spans' number is greatly affected (double), that due to the contribution of the catenary *L2*, which produced the same magnetic-field intensity as the original span (*L*) in this case as explained in Fig. 3, and, of course, the catenary *L1* have a small contribution in the calculated values of the magnetic-field intensities in this case.

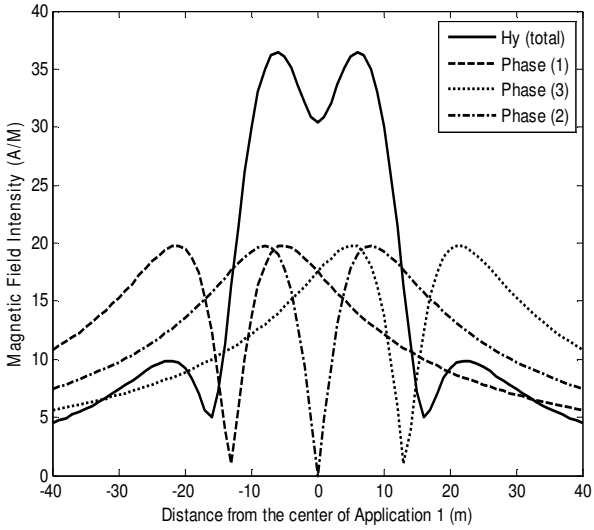

Fig. 8. Contribution of each phase in the Y-component of the magnetic-field intensity.

Tables 1(a) and 1(b) present the effect of the number of spans (*N*) on the calculated magnetic-field intensity, it was seen that as the number of the spans is greater than 5 (*N* is greater than 2), the result of the calculated magnetic-field intensity is nearly the same, that due to the far distances between the current source points and the field points. For this reason, the number of spans does not exceed 5 (*N*=2).

Adel Z. EL Dein

JOURNAL OF PHYSICS VOL. 1 NO. 2 July (2012) PP. 11 - 23

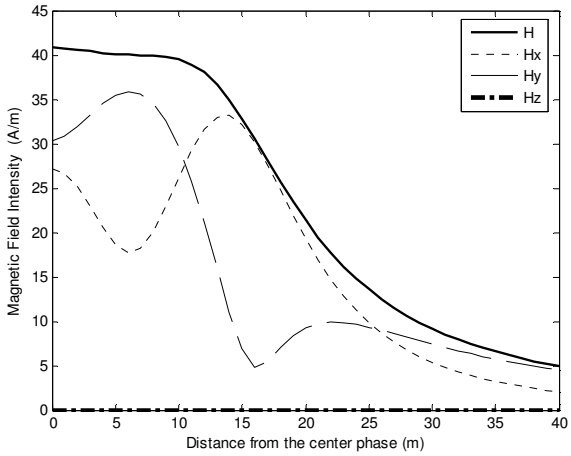

Fig. 9. Computed magnetic-field intensity by using the 3-D integration technique (point P1).

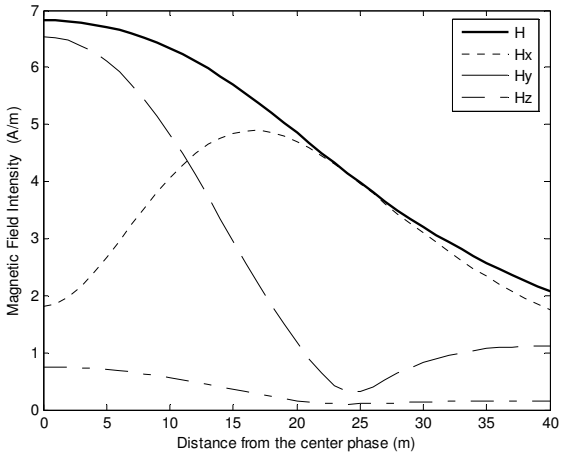

Fig. 10. Computed magnetic-field intensity by using the 3-D integration technique (point P2).

Table 1(a)
Effect of the Number of Spans on the Magnetic-field Intensity Calculated by 3-D Integration Technique

Distance from the center phase (m)	Magnetic-field Intensity (A/m) calculated by 3-D Integration technique			
	Cross-section P2			
	N=0 Single Span	N=1 No. of spans=3	N=2 No. of spans=5	N=3 No. of spans= 7
0	6.825	13.57	13.586	13.588
10	6.338	12.632	12.64	12.641
20	4.853	9.701	9.703	9.704
30	3.202	6.396	6.393	6.393
40	2.081	4.145	4.14	4.139

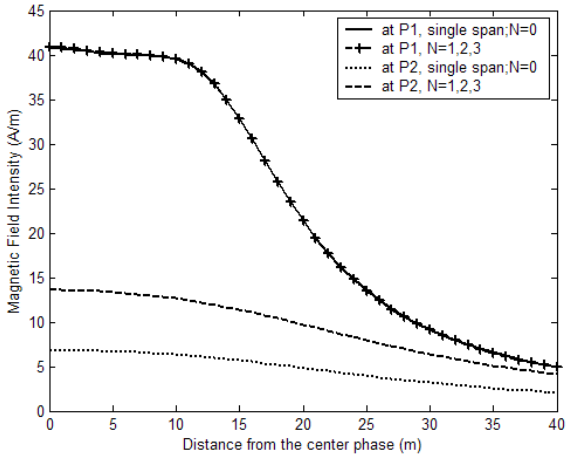

Fig. 11. Effect of the spans' numbers on the magnetic-field intensity.

Fig. 12 shows the effect of the angle θ as explained in case (B) on the calculated magnetic-field intensity of a single span under a tower height (point P2 in Fig.4) and a distance away from the center phase. It is seen that as the angle θ increased, the magnetic-field intensity decreased due to the increases of the distance between the current source and the field points. Fig. 13 shows the same results as in Fig. 12, except that the calculation points are at midspan (point P3 in Fig. 4) and a distance away from the center phase. It is noticed that the effect of angle θ is higher in this case because all the current-source points on the catenary *L2* are far from the field points since the angle θ increased.

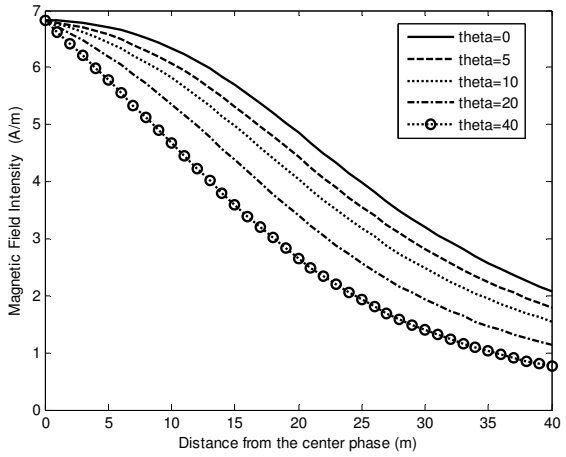

Fig. 12. Effect of the angle θ on the magnetic-field intensity calculated under tower height.

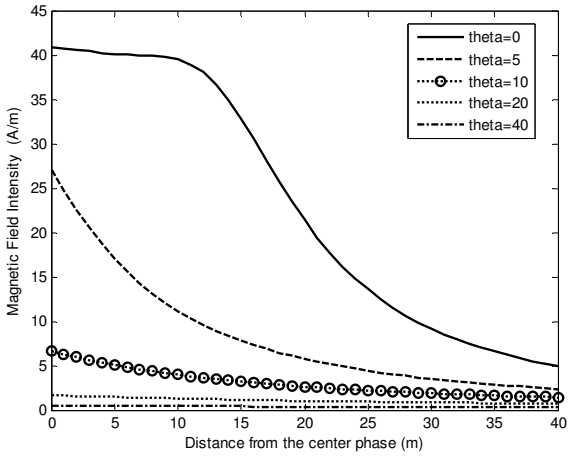

Fig. 13. Effect of the angle θ on the magnetic-field intensity calculated under mid-span.

Table 1(b)
Effect of the Number of Spans on the Magnetic-field Intensity Calculated by 3-D Integration Technique

Distance from the center phase (m)	Magnetic-field Intensity (A/m) calculated by 3-D Integration technique			
	Cross-section P1			
	N=0 Single Span	N=1 No. of spans=3	N=2 No. of spans=5	N=3 No. of spans=7
0	40.796	40.865	40.871	40.872
10	39.5	39.546	39.551	39.552
20	21.38	21.344	21.341	21.34
30	9.163	9.101	9.095	9.094
40	4.958	4.892	4.885	4.884

Tables 2 and 3 present a comparison between the magnetic-field intensity calculated with both 2-D straight line technique, where the average conductors' heights are used, and 3-D integration technique, with various angles θ, various span lengths, and various differences between the towers' heights, are taken into account, that at both tower height (point P2) and midspan (point P1) and a distance away from the center phase, respectively. From both two Tables, it is seen that the difference between the towers' heights have a small effect, when the magnetic-field intensity is calculated at the tower height, but when the magnetic-field intensity is calculated at midspan, it has a greater effect, especially when this difference is equal to the sag itself.

From Tables 2 and 3 and Figs. 8, 9 and 10, it is seen that there are large differences between the values of the magnetic-field intensity computed by using the traditional 2-D straight-line technique and the 3-D integration technique (θ=0, LL=0 and L=400m). That is due to the variation of the conductors' heights over the field pints, whereas in 2-D straight line technique, the conductors' heights are always assumed equal to average height (h+1/3 of sag), which is higher than the minimum conductor height (h), hence 2-D straight line technique produced a magnetic-field intensity that is smaller than that calculated by 3-D integration technique under midspan as indicated in Table 3 and Figs. 8 and 9. Also, the average height is smaller than the maximum conductor height (h_m), hence 2-D straight line technique produced a magnetic-field intensity greater than that calculated by 3-D integration technique under maximum conductor height as indicated in Table 4 and Figs. 8 and 10.

Table 2
Comparison Between The Results Of 3-D Integration Technique With Various Parameters At Tower Height And 2-D Straight-Line Technique

Distance from the center phase (m)	2-D straight line technique with average heights (A/m)	3-D integration technique Single span at point P2 (tower height) (A/m)								
		Angle (θ) (deg.) With : L=400m, LL=0m			Span (L) (m) With : θ =0deg, LL=0m			Different between towers' heights (LL) (m); With : θ =0deg, L=400m		
		θ=0	θ=10	θ=40	L=400	L=350	L=300	LL=0	LL=10	LL=S
0	25.236	6.824	6.824	6.824	6.824	6.721	6.666	6.824	6.808	6.792
10	23.619	6.337	5.817	4.674	6.337	6.234	6.179	6.337	6.324	6.313
20	15.218	4.852	4.044	2.660	4.852	4.77	4.725	4.852	4.849	4.846
30	7.957	3.202	2.482	1.399	3.202	3.154	3.128	3.202	3.207	3.210
40	4.584	2.081	1.547	0.765	2.081	2.055	2.042	2.081	2.090	2.097

Table 3
Comparison Between the Results of 3-D Integration Technique with Various Parameters at midspan and 2-D Straight Line Technique

Distance from the center phase (m)	2-D straight line technique with average heights (A/m)	3-D integration technique Single span at point P1 (mid-span) (A/m)								
		Angle (θ)(deg) With : L=400m, LL=0m			Span (L) (m) With : θ =0deg, LL=0m			Different between towers' heights (LL) (m); With : θ =0deg, L=400m		
		θ=0	θ=10	θ=40	L=400	L=350	L=300	LL=0	LL=10	LL=S
0	25.236	40.796	6.690	0.476	40.796	29.22	23.946	40.796	40.335	20.398
10	23.619	39.499	3.953	0.422	39.499	27.361	22.118	39.499	39.152	19.750
20	15.218	21.381	2.624	0.375	21.381	16.809	14.441	21.381	21.534	10.691
30	7.957	9.164	1.877	0.335	9.164	8.347	7.785	9.164	9.357	4.582
40	4.584	4.959	1.414	0.300	4.959	4.742	4.583	4.959	5.061	2.479

I. Application of the Suggested Technique

In general, by using the discussed three cases (A, B, and C) and the superposition technique, one can calculate the magnetic-field intensity at any field point from any number of catenaries of various configurations.

Consider the following suggested general case which is presented in Fig. 14, and in which the power transmission lines are specified by, unequal heights of the towers, unequal spans between towers and the power transmission lines' spans that are not parallel to each others. Fig. 15 presents the single line diagram of the suggested case 500-kV overhead transmission line, its equivalent straight line and the calculation lines (applications 1, 2 and 3). Table 4 presents the parameters which describe the overhead transmission line.

The calculation of the magnetic-field intensity at any field point on the application 1 (Fig. 16) can be done as follows:

1- When the field point is located in the same coordinate system of the catenary under consideration, equations of case (A) are used if the catenary has tower that are of equal heights (e.g. as span 7), and equations of case (C) are used if the catenary has towers that are of unequal heights (e.g. as span 8).
2- When the field point is located in coordinate system makes an angle θ with the coordinate system of the catenary under calculation, equations of case (B) are used when the catenary has tower of equal heights (e.g. as spans 1,4,5 and 6), and also the equations of case (B) are used when the catenary has towers of unequal heights, but in this case α, and the limits of the integration are the same as those of case (C) (e.g. as spans 2 and 3).

The same rules can be used to calculate the magnetic-field intensity at any field point on the applications 2 and 3, the only required is the angle between the field point coordinate system and each span coordinate system.

Table 4
Classification of the suggested case spans

Span number	Angle θ in degrees	Span length (m)	Heights of span two ends (m)
1	70	400	h_m and h_m
2	75	450	h_m and (h_m +5m)
3	40	400	(h_m +5m) and h_m
4	20	400	h_m and h_m
5	15	400	h_m and h_m
6	5	400	h_m and h_m
7	0	400	h_m and h_m
8	0	400	h_m and (h_m+5m)

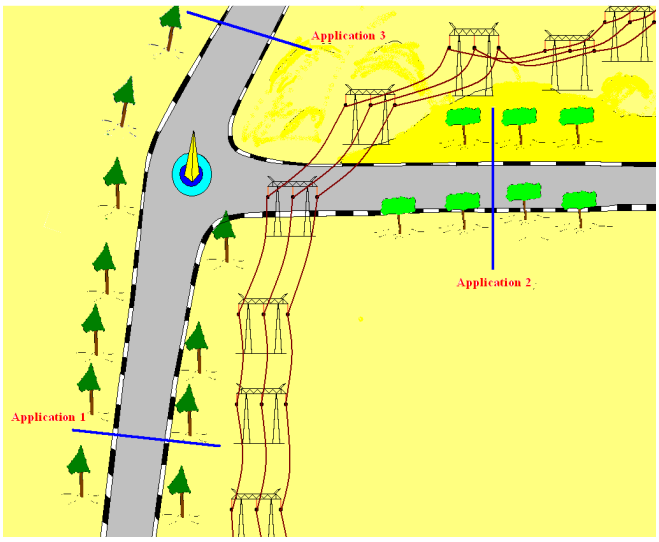

Fig. 14. Suggested case study of a single circuit 500-kV overhead transmission line.

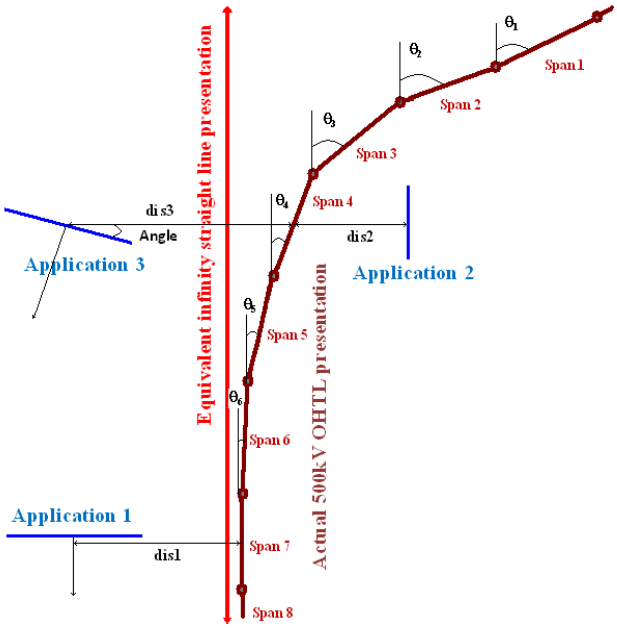

Fig. 15. Single line diagram of the suggested case.

Fig. 16 shows the comparison between the results of 3-D integration technique and 2-D straight line, when they are applied on the field points of the application 1, with various distances between center of application 1 and the span 7 (dis1 in Fig. 15). It is noticed that the magnetic-fields from 3-D integration technique are greeter than those from 2-D straight line, and the maximum difference is under the center of the overhead transmission line. Also it is noticed that as the distance (dis1 in Fig. 15) increases the point of maximum magnetic-field goes far from the center of application 1 and toward the transmission line. Fig. 16 shows the comparison between the results of 3-D integration technique and 2-D straight line, when they are applied on the field points of the application 2, with various distances between center of application 2 and the span 4 (dis2 in Fig. 15). It is noticed that the magnetic-fields from 3-D integration technique are greeter than those from 2-D straight line, and the maximum difference is under the center of the overhead transmission line. Also it is noticed that as the distance (dis2 in Fig. 15) increases the point of maximum magnetic-field goes far from the center of application 2 and toward the transmission line.

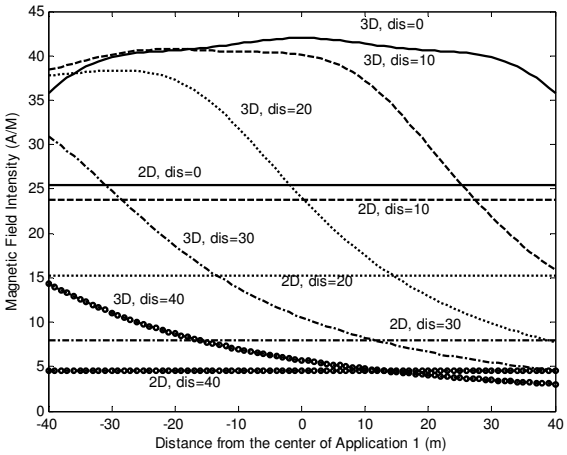

Fig. 16. Computed magnetic-field intensity by using the 3-D integration technique and 2-D straight line with various distances from the overhead transmission line at application 1.

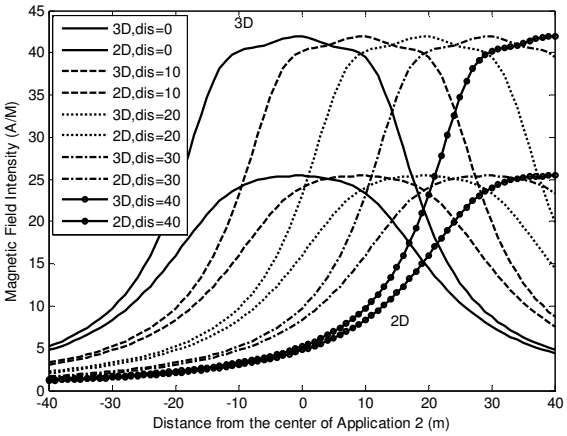

Fig. 17. Computed magnetic-field intensity by using the 3-D integration technique and 2-D straight line with various distances from the overhead transmission line at application 2.

Fig. 18 shows the comparison between the results of 3-D integration technique and 2-D straight line, when they are applied on the field points of the application 3, with various distances between center of application 3 and the span 4 (dis3 in Fig. 15). It is noticed that the magnetic-fields from 3-D integration technique are greeter than those from 2-D straight

line, and the maximum difference is under the center of the overhead transmission line. Also it is noticed that as the distance (dis3 in Fig. 15) increases the point of maximum magnetic-field goes far from the center of application 3 and toward the transmission line. Fig. 19 shows the comparison between the results of 3-D integration technique and 2-D straight line, when they are applied on the field points of the application 3, with various angles between application 3 and horizontal line (angle in Fig. 15). It is noticed that the magnetic-fields from 3-D integration technique are greeter than those from 2-D straight line, and the maximum difference is under the center of the overhead transmission line.

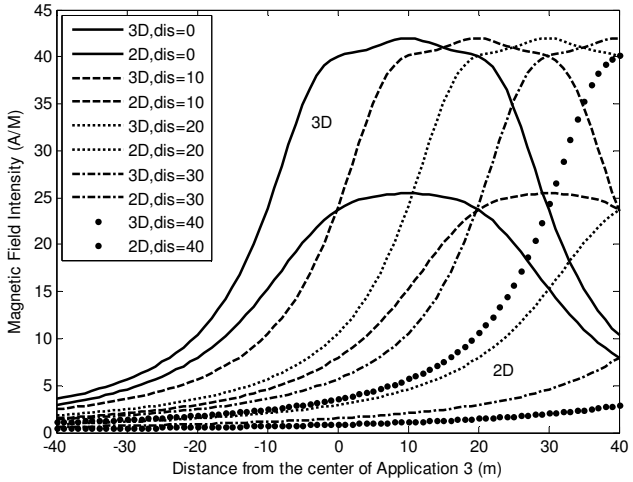

Fig. 18. Computed magnetic-field intensity by using the 3-D integration technique and 2-D straight line with various distances from the overhead transmission line at application 3.

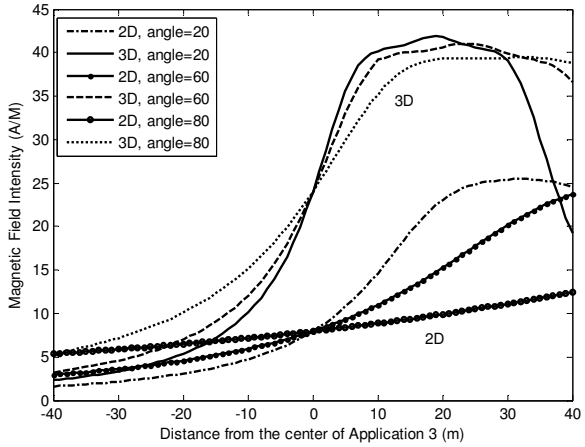

Fig. 19. Computed magnetic-field intensity by using the 3-D integration technique and 2-D straight line with various angles of application 3.

II. CONCLUSIONS

The 2-D straight line and 3-D integration techniques give two choices for calculating magnetic-field. The 2-D Straight Line is a rough approximation, and the 3-D integration is an exact solution, however it requires integration over the three-phase spans which results in long computation time. It is seen that by using the 3-D integration technique, the Z-component of the magnetic-field intensity appears, whereas this component is always equal to zero in the 2-D straight-line technique. Under the 3-D integration technique, this paper presents multispecial cases to calculate the magnetic-field intensity, by using these cases, it is possible to calculate the magnetic-field intensity at any point under complex configurations of power transmission lines, as was explained in this paper on the suggested case study. Also, it is possible to use the same technique, with some treatment, in the calculation of the electric field under overhead transmission lines.

REFERENCES

[1] W. T. Kaune and L. E. Zaffanella, “Analysis of magnetic-fields produced far from electric power lines” IEEE Transactions on Power Delivery, Vol. 7, No. 4, October 1992, pp. 2082-2091.

[2] R. G. Olsen and P. Wong, “Characteristics of Low Frequency Power Lines” IEEE Transactions on Power Delivery, Vol. 7, No. 4, October 1992, pp. 2046-2053.

[3] M. L. Pereira Filho, J. R. Cardoso, C. A. F. Sartori, M. C. Costa, B. P. de Alvarega, A. B. Dietrich, L. M. R. Mendes, I. T. Domingues and J. C. R. Lopes “ Upgrading Urban High Voltage Transmission Line: Impact on Electric and Magnetic-fields in the Environment” 2004 IEEE/PES Transmission and Distribution Conference and Exposition: Latin America, pp 788-793

[4] Hanaa Karawia, Kamelia Youssef and Ahmed Hossam-Eldin "Measurements and Evaluation of Adverse Health Effects of Electromagnetic-fields from Low Voltage Equipments" MEPCON 2008, Aswan, Egypt, March 12-15 ,PP. 436-440.

[5] Ahmed A, Hossam-Eldin and Wael Mokhtar "Interference Between HV Transmission Line And Nearby Pipelines" MEPCON 2008, Aswan, Egypt, March 12-15 ,PP. 218-223

[6] George Filippopoulos, and Dimitris Tsanakas " Analytical Calculation of the Magnetic-field Produced by Electric Power Lines" IEEE Transactions on Power Delivery, Vol. 20, No. 2, pp. 1474-1482, April 2005.

[7] Federico Moro and Roberto Turri “ Fast Analytical Computation of Power-Line Magnetic-fields by Complex Vector Method” IEEE Transactions on Power Delivery, Vol. 23, No. 2, October 2008, pp. 1042-1048.

[8] A. A. Dahab, F. K. Amoura, and W. S. Abu-Elhaija "Comparison of Magnetic-Field Distribution of Noncompact and Compact Parallel Transmission-Line Configurations" IEEE Transactions on Power Delivery, Vol. 20, No. 3, pp. 2114-2118, July 2005.

[9] A. V. Mamishev, R. D. Nevels, and B. D. Russell "Effects of Conductor Sag on Spatial Distribution of Power Line

Magnetic-field" IEEE Transactions on Power Delivery, Vol. 11, No. 3, pp. 1571-1576, July 1996.

[10] Rakosk Das Begamudre,"Extra High Voltage AC. Transmission Engineering" third Edition, Book, Chapter 7, pp.172-205, 2006 Wiley Eastern Limited.

[11] H. M. Ismail, "Magnetic Field Analysis of the Egyptian High Voltage Transmission Networks Using the Vector Magnetic Potential Concept", Scientific Bulletin, Faculty of Engineering, Ain Shams University, vol. 41 (Part 2) 2006, pp. 513-526.

[12] H. M. Ismail, "Magnetic Field Calculations and Management of Kuwait HVTLs Using the Vector Magnetic Potential Concept", Proceedings of the IEEE Power Tech'99 Conference, Budapest, Hungary, Paper BPT99-122-51, 1999.

[13] Adel Z. El Dein, "Magnetic Field Calculation under EHV Transmission Lines for More Realistic Cases", IEEE Transactions on Power Delivery, VOL. 24, NO. 4, October 2009, PP. 2214-2222.

Appendix (A)

Assume two coordinates' systems (X,Y,X) and (U,V,W) in a space, where axis U and axis W in system (U,V,W) form an angle θ with axis X and axis Z in system (X,Y,Z) respectively, while axis V and axis Y are parallel to each other, and the original of the system (U,V,W) located at point (x_c,y_c,z_c) refers to system (X,Y,Z), as indicated in Fig. 19. Any point P in space can be presented by the two system as (x_1,y_1,z_1) in system (X,Y,Z) and (u_1,v_1,w_1) in system (U,V,W).

From Fig. A.1, the following is seen:

$$L`` = \frac{w_1}{\sin(\beta)} \quad \text{(A.1)}$$

$$L`` = \frac{u_1}{\cos(\beta)} \quad \text{(A.2)}$$

$$zz = L`` \sin(\beta+\theta) \quad \text{(A.3)}$$

$$xx = L`` \cos(\beta+\theta) \quad \text{(A.4)}$$

$$zz = z_1 - z_c \quad \text{(A.5)}$$

$$xx = x_1 - x_c \quad \text{(A.6)}$$

$$z_1 = z_c + zz \quad \text{(A.7)}$$

$$x_1 = x_c + xx \quad \text{(A.8)}$$

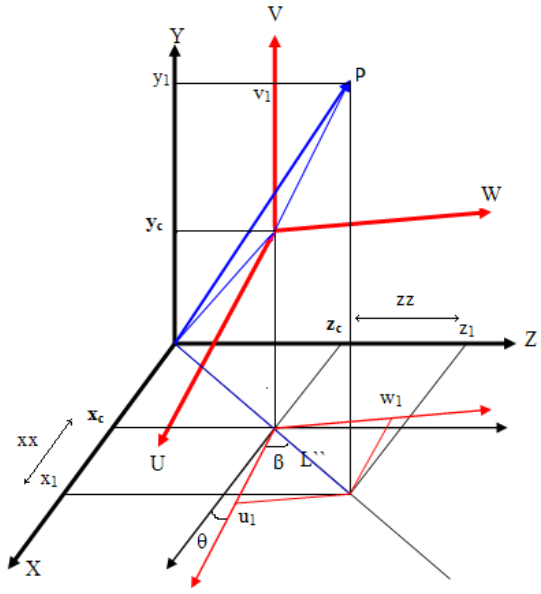

Fig. A.1 The cartesian coordinates of two systems in space

A1: To transfer any point (u_1,v_1,w_1) in the (U,V,W) system to a point (x_1,y_1,z_1) in the (X,Y,Z) system;

By substituting (A.3) and (A.1) into (A.7):

$$z_1 = z_c + \frac{w_1}{\sin(\beta)} \sin(\beta+\theta) \quad \text{(A.9)}$$

By substituting (A.4) and (A.2) into (A.8):

$$x_1 = x_c + \frac{u_1}{\cos(\beta)} \cos(\beta+\theta) \quad \text{(A.10)}$$

and; $y_1 = y_c + v_1$ (A.11)

where: $\beta = \tan^{-1} \frac{w_1}{u_1}$ (A.12)

A2: To transfer any point (x_1,y_1,z_1) in the (X,Y,Z) system to a point (u_1,v_1,w_1) in the (U,V,W) system;

By substituting (A.3) and (A.5) into (A.1):

$$w_1 = \frac{z_1 - z_c}{\sin(\beta+\theta)} \sin(\beta) \quad \text{(A.13)}$$

By substituting (A.4) and (A.6) into (A.2):

$$u_1 = \frac{x_1 - x_c}{\cos(\beta+\theta)} \cos(\beta) \quad \text{(A.14)}$$

and; $v_1 = y_1 - y_c$ (A.15)

where: $\beta = \tan^{-1} \frac{zz}{xx} - \theta = \tan^{-1} \frac{z_1 - z_c}{x_1 - x_c} - \theta$ (A.16)

Appendix (B)

To calculate the magnetic-field intensity under 500-kV transmission line single circuit, the data in Table B.1 are used.

Table B.1
Data of 500-kV Overhead Transmission Line

Tower span (L)	400m
Number of subconductor per phase (n)	3
Diameter of a subconductor (2r)	30.6mm
Spacing between subconductors (B)	45cm
Minimum clearance to ground (h)	9m
Outer phase Maximum height ($h_m=H_{outer}$)	22m
Inner phase Maximum height ($h_m=H_{inner}$)	24.35m
Distance between adjacent two phases (D)	13.2m

Adel Z. El Dein *was born in Egypt 1971. He received the B.Sc., M. Sc. degrees in electric engineering from the Faculty of Energy Engineering, Aswan, Egypt, in 1995 and 2000, respectively, and the Ph. D. degree in electric engineering from Kazan State Technical University, Kazan, Russia in 2005. His fields of interest include electric and magnetic-fields and their effects, comparison of numerical techniques in electromagnetics, design of microstri antennas and filters, and the calculation of specific absorption rate in Human body.*